Optical measurement of thermal transport in suspended carbon nanotubes

I-Kai Hsu, Rajay Kumar, Adam Bushmaker, and Stephen B. Cronin[a)]
Department of Materials Science and Electrical Engineering, University of Southern California, Los Angeles, California 90089, USA

Michael T. Pettes and Li Shi
Department of Mechanical Engineering and Center for Nano and Molecular Science and Technology, Texas Materials Institute, University of Texas of Austin, Austin, Texas 78712, USA

Todd Brintlinger, Michael S. Fuhrer, and John Cumings
Department of Physics and Center for Superconductivity Research and Department of Materials Science and Engineering, University of Maryland, College Park, Maryland 20742, USA

(Received 30 September 2007; accepted 8 December 2007; published online 15 February 2008)

Thermal transport in carbon nanotubes is explored using different laser powers to heat suspended single-walled carbon nanotubes ~5 μm in length. The temperature change along the length of a nanotube is determined from the temperature-induced shifts in the *G* band Raman frequency. The spatial temperature profile reveals the ratio of the contact thermal resistance to the intrinsic thermal resistance of the nanotube. Moreover, the obtained temperature profiles allow differentiation between diffusive and ballistic phonon transport. Diffusive transport is observed in all nanotubes measured and the ratio of thermal contact resistance to intrinsic nanotube thermal resistance is found to range from 0.02 to 17. © *2008 American Institute of Physics*. [DOI: 10.1063/1.2829864]

Thermal transport in carbon nanotubes has stimulated a great deal of interest due to the exceptionally high thermal conductivity predicted theoretically[1–4] and observed experimentally.[5–11] The thermal conductivity of single-walled (SW) and multiwalled (MW) carbon nanotubes (CNTs) depends on diameter and temperature and has been measured and simulated in the range of 250–6600 W/m K[1,2,7,10,12] and 300–3000 W/m K,[5,8,11] respectively. Measuring the thermal conductivity of nanotubes presents several challenges, including the uncertainty in the thermal contact resistance, difficulty in generating and accurately determining temperature gradients over very short lengths, and large variations in nanotube quality. Additionally, nanotubes' low-dimensional nature makes them especially sensitive to defects and slight perturbations of their geometries.

Individual MWCNTs and SWCNTs suspended between microfabricated heaters have been measured, yielding room-temperature thermal conductivities above 2500 W/m K.[5,7] Chiu *et al.*, using a self-heating approach, determined the high-temperature thermal conductivity of MWCNTs from electron transport measurements to be 600 W/m K.[13] Fujii *et al.*[8] and Chang *et al.*[9] reported that the room-temperature thermal conductivity of MWCNTs increases with decreasing diameter to exceed 2000 and 1000 W/m K, respectively. By fitting the electron transport data with a Joule self-heating model, Pop *et al.* obtained thermal conductivities of suspended SWCNTs of nearly 3500 W/m K.[12] Discrepancies between various measurements in the literature are likely due to differences in nanotube quality and thermal contact resistance, which cannot be excluded from the measurement results by any of the existing methods. Moreover, the contribution of contact thermal resistance to the thermal measurement prevents one from establishing whether phonon transport in several micron-long nanotubes is ballistic or diffusive. Reliable techniques for investigating thermal transport in nanotubes, especially the contact thermal resistance and the ballistic or diffusive phonon transport nature, are much needed.

In this study, we present a technique for better understanding thermal transport in nanotubes using an optical, noncontact method. This method reveals the ratio between the contact and the intrinsic thermal resistance of the nanotube, and also differentiates between diffusive and ballistic phonon transport.

In our experiment, SWCNTs are grown suspended over ~5 μm trenches etched in a Si/SiO_2 substrate by chemical vapor deposition.[14,15] A 532 nm Spectra-Physics solid state laser is collimated and focused through a Leica DM LM microscope. A 100× objective lens with a numerical aperture of 0.9 produces a 0.36 μm diameter laser spot. Raman spectra are measured in a Renishaw inVia Raman microspectrometer. Only nanotubes that are strongly resonant with the laser energy are used for heating in this study.[16] The temperature-induced downshifts of the *G* band were calibrated in a Linkam THMSE 600 temperature controlled stage. The position of the laser spot along the length of the nanotube was determined relative to the edge of the trench using a high precision Prior ProScan II microscope stage.

Figure 1(a) shows a scanning electron microscopy (SEM) image of a SWCNT suspended across a 4.7 μm trench. The radial breathing mode (RBM) of this nanotube was observed at 147 cm^{-1}, implying a nanotube diameter of 1.66 nm by the relation $\omega_{RBM}=223.5/d_t+12.5$.[17] The radial breathing mode was only observed in one of the nanotubes measured in this work, thus precluding the (n,m) assignments of other nanotubes. While we are unable to demonstrate a metallic/semiconductor dependence on the thermal conductivity, electrons are not expected to make a significant contribution to thermal transport in CNTs.[7,18,19] The size and location of the laser spot where spectra were taken is indicated in this figure by the white circles. Figure 1(b) shows

[a)]Electronic mail: scronin@usc.edu.

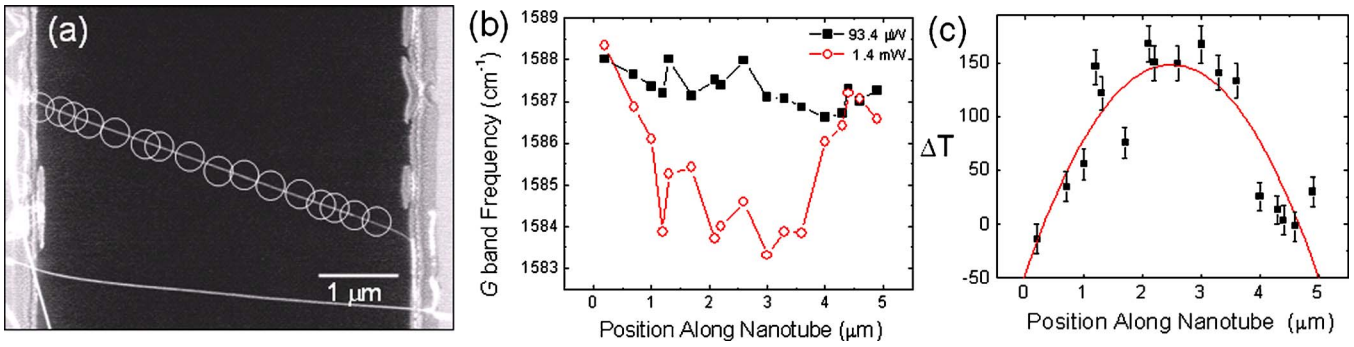

FIG. 1. (Color online) (a) SEM image of carbon nanotubes suspended over a 4.7 μm trench. (b) G band Raman frequency measured along the length of the nanotube in (a) at different laser powers. (c) Laser heating profile of the suspended nanotube shown in Fig. 1(a). Error bars reflect the uncertainties in the G band shift and its temperature coefficient.

the corresponding results of Raman spectra measured at lower laser power (93 μW) and higher laser power (1.4 mW) at these designated locations. The G band consists of two peaks that both downshift with temperature. We typically use the higher component (G_+) in these temperature-dependent studies simply because it has a sharper linewidth and a higher intensity. Figure 1(b) shows the G band Raman frequencies measured at 17 points along the suspended nanotube at these two laser powers. We observe larger downshifts in the center of the suspended nanotube than at the ends, which are thermally heat sunk to the Si/SiO_2 substrate. Because of the G band's strong sensitivity to changes in temperature,[20–22] we can relate the observed changes in the G band frequency to changes in the nanotube temperature.The measured temperature coefficient of the G band displays a linear temperature dependence with a slope of $-0.022\ cm^{-1}/K$,[23] which is consistent with previous measurements in the literature. After converting the changes in G band frequency into temperature changes[24,25], we are able to determine the local temperature rise $\Delta T(x)$ as a function of the position x of the incident laser spot which can be fitted with a 2nd order polynomial to be $\Delta T(x) = -31x^2 + 155x - 43$, where ΔT is in Kelvin and x is in micrometers.

If the phonon transport in a nanotube is diffusive, we can solve the Fourier heat equation for one-dimensional heat transport. For the current experiment, the total heat generation rate ($\dot{Q}$) by the incident laser is equal to the sum of the heat flow rates to the right and left hand sides of the nanotube, which is $\dot{Q} = \dot{Q}_{\text{left}} + \dot{Q}_{\text{right}} = \Delta T/[x/(\kappa A) + R_{c,\text{left}}] + \Delta T/[(L-x)/(\kappa A) + R_{c,\text{right}}]$, where κ is the nanotube thermal conductivity, L and A are the length and geometric cross section of the suspended nanotube, x is the distance of the laser spot from the left edge of the trench, and $R_{c,\text{left}}$ and $R_{c,\text{right}}$ are the contact thermal resistances at the two ends of the nanotube. The measured temperature profile along the nanotube can be obtained by solving for ΔT, as $\Delta T(x) = \dot{Q}[-x^2/(\kappa A)^2 + x(L/(\kappa A)^2 + (R_{c,\text{right}} - R_{c,\text{left}})/\kappa A) + R_{c,\text{right}}R_{c,\text{left}} + L/(\kappa A)R_{c,\text{left}}]/[L/(\kappa A) + R_{c,\text{left}} + R_{c,\text{right}}]$. This complicated looking but otherwise simple algebraic expression reduces to $\Delta T(x) = \dot{Q}/\kappa AL(-x^2 + Lx)$, when the two contact thermal resistances are negligible compared to the intrinsic thermal resistance of the nanotube $R_{\text{NT}} = L/\kappa A$. The resulting temperature profile, predicted by this model, is a parabola with negative curvature given by $\dot{Q}/\kappa AL$, which is what we observe in Fig. 1(c).

Figure 2 shows the results of laser heating of a different nanotube, in which the thermal contact resistance is much larger than the thermal resistance of the nanotube itself. The temperature profile shows a linear and asymmetric region in the central part of the nanotube. ΔT at the left and right ends of this linear region are approximately 50 and 100 K, respectively, indicating a large contact resistance with $R_{c,\text{right}} > R_{c,\text{left}}$.

For large $R_{c,\text{right}}$ or $R_{c,\text{left}}$, the curvature of $\Delta T(x)$, given by $2\dot{Q}(\kappa A)^{-2}(L/\kappa A + R_{c,\text{left}} + R_{c,\text{right}})^{-1}$, becomes very small, resulting in the nearly linear slope observed in Fig. 2. According to the equation for $\Delta T(x)$, the ratio of temperature rises at the two ends of the nanotube is $\Delta T(L)/\Delta T(0) = [R_{c,\text{right}}(R_{c,\text{left}} + R_{\text{NT}})]/[R_{c,\text{left}}(R_{c,\text{right}} + R_{\text{NT}})]$. Figure 2 shows that this ratio is about 2. This value of 2 can be caused by a $R_{c,\text{right}}$ value much larger than $R_{c,\text{left}}$ that is comparable to R_{NT}. In this case, the total contact thermal resistance is much larger than R_{NT}. Therefore, the contact regions of the nanotube, especially the right contact, act as a phonon bottleneck. The deviations from linearity at the ends of the nanotube are due to the strongly absorbing substrate, which is normally not in the focal volume of the laser spot. This substrate absorption causes additional heating, which results in an increase in temperature as the laser is brought near the edges of the trench. Moreover, if the phonon transport were ballistic in this sample, the temperature rise would result in a constant

TABLE I. Summary of the temperature rise profile measurements of four suspended nanotubes.

Sample	a ($K/\mu m^2$)	b ($K/\mu m$)	c (K)	Length (μm)	P_{laser} ($mW/\mu m^2$)	$R_{c,\text{left}}/R_{\text{NT}}$	$R_{c,\text{right}}/R_{\text{NT}}$
1	31	155	<15	5.0	13	0.02	0.02
2	48	118	27	2.6	16	0.08	0.08
3	<0.2	16	26	5.0	25	0.32	17
4	3.6	−7.9	144	4.7	3.1	1.59	0.13

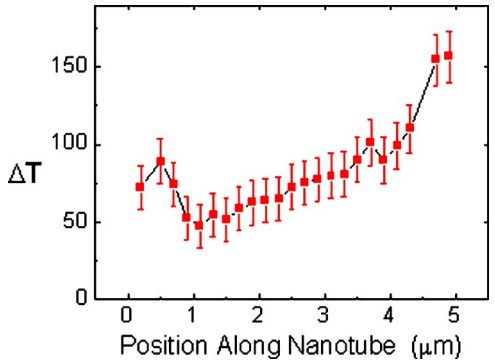

FIG. 2. (Color online) Temperature increase profile along a suspended nanotube, as determined from the G band downshifts measured with 365 μW and 2.87 mW laser power. Error bars are as in Fig. 1.

$\Delta T(x)$ regardless of asymmetric contact resistance. Hence, the linear slope of the temperature profile indicates that phonon transport in this sample is also diffusive.

We performed a systematic study of the temperature increase profile $\Delta T(x)$ of four different nanotubes using this laser heating method. These results are summarized in Table I. While we are unable to determine the amount of heat generated in the nanotubes by the laser ($\dot{Q}$), we can determine the ratio between the contact and nanotube thermal resistances, $r_l \equiv R_{c,\mathrm{left}}/R_{\mathrm{NT}}$ and $r_r \equiv R_{c,\mathrm{right}}/R_{\mathrm{NT}}$. We express temperature change along the suspended carbon nanotube in the general form of $\Delta T(x) = -ax^2 + bx + c$ and define the following coefficient ratios $\alpha = b/a = L(1 - r_l + r_r)$ and $\beta = c/a = L^2 r_l (1 + r_r)$. The ratios between the contact and nanotube thermal resistances are then given by $r_l \equiv R_{c,\mathrm{left}}/R_{\mathrm{NT}} = (-\alpha + \sqrt{\alpha^2 + 4\beta})/(2L)$ and $r_r \equiv R_{c,\mathrm{right}}/R_{\mathrm{NT}} = -1 + (\alpha + \sqrt{\alpha^2 + 4\beta})/(2L)$.

For the extreme cases of negligible contact resistance and negligible nanotube resistance, we estimate upper limits for the curvature (a) and offset (c) of the temperature profile from the experimental uncertainty. These are indicated in Table I by the $<$ signs. Samples 1 and 3, in the table, correspond to the data shown in Figs. 1(c) and 2, respectively. The laser power density (P_{laser}), used to heat the suspended nanotubes, is also indicated in the table. The values of $R_{c,\mathrm{left}}/R_{\mathrm{NT}}$ and $R_{c,\mathrm{right}}/R_{\mathrm{NT}}$ span the range from 0.02, for negligible contact resistance, to 17, for the case of dominant contact resistance. The large variability in R_c/R_{NT} is attributed to the variation in nanotube quality and quality of the thermal contact to the substrate. Sample 3 exhibits a thermal contact resistance far exceeding that of the other samples. The origin of this large thermal contact resistance is unknown. There were no visible differences observed in the SEM images or Raman spectra (including the D-band/G-band intensity ratio) of this nanotube.

In conclusion, a noncontact method for observing thermal transport in individual carbon nanotubes is demonstrated. By spatially resolving the temperature rise profile along the length of nanotubes, this technique can determine the influence of thermal contact resistance and distinguish between diffusive and ballistic transport. Distinct behaviors of the temperature rise profile $\Delta T(x)$ are attributed to the thermal contact resistance and that of the nanotube itself. The ratios of the thermal contact resistance to the thermal resistance of the nanotube span the range from 0.02 to 17. All results indicate that phonon transport in these nanotubes is diffusive or that the phonon mean free path is shorter than the 2.6–5 μm suspended length of the nanotube. As such, thermal transport in the four nanotubes can be explained with a simple Fourier heat transport model.

This research was supported in part by DOE Award Nos. DE-FG02-07ER46376 and DE-FG02-07ER46377, the James H. Zumberge Fund, the Powell Foundation, and the National Science Foundation Graduate Research Fellowship Program.

[1] S. Berber, Y. K. Kwon, and D. Tomanek, Phys. Rev. Lett. **84**, 4613 (2000).
[2] S. Maruyama, Physica B **323**, 193 (2002).
[3] X. H. Yan, Y. Xiao, and Z. M. Li, J. Appl. Phys. **99**, 124305 (2006).
[4] N. Mingo and D. A. Broido, Phys. Rev. Lett. **95**, 096105 (2005).
[5] P. Kim, L. Shi, A. Majumdar, and P. L. McEuen, Phys. Rev. Lett. **87**, 215502 (2001).
[6] J. Hone, M. C. Llaguno, N. M. Nemes, A. T. Johnson, J. E. Fischer, D. A. Walters, M. J. Casavant, J. Schmidt, and R. E. Smalley, Appl. Phys. Lett. **77**, 666 (2000).
[7] C. H. Yu, L. Shi, Z. Yao, D. Y. Li, and A. Majumdar, Nano Lett. **5**, 1842 (2005).
[8] M. Fujii, X. Zhang, H. Q. Xie, H. Ago, K. Takahashi, T. Ikuta, H. Abe, and T. Shimizu, Phys. Rev. Lett. **95**, 065502 (2005).
[9] C. W. Chang, A. M. Fennimore, A. Afanasiev, D. Okawa, T. Ikuno, H. Garcia, D. Y. Li, A. Majumdar, and A. Zettl, Phys. Rev. Lett. **97**, 085901 (2006).
[10] J. Hone, M. Whitney, C. Piskoti, and A. Zettl, Phys. Rev. B **59**, R2514 (1999).
[11] T. Y. Choi, D. Poulikakos, J. Tharian, and U. Sennhauser, Nano Lett. **6**, 1589 (2006).
[12] E. Pop, D. Mann, Q. Wang, K. Goodson, and H. J. Dai, Nano Lett. **6**, 96 (2006).
[13] H. Y. Chiu, V. V. Desphande, H. W. C. Postma, C. N. Lau, C. Miko, L. Forro, and M. Bockrath, Phys. Rev. Lett. **95**, 226101 (2005).
[14] T. H. Brintlinger, PhD Thesis, University of Maryland, p. 139, 2005.
[15] J. Kong, H. T. Soh, A. M. Cassell, C. F. Quate, and H. J. Dai, Nature (London) **395**, 878 (1998).
[16] A. Jorio, R. Saito, J. H. Hafner, C. M. Lieber, M. Hunter, T. McClure, G. Dresselhaus, and M. S. Dresselhaus, Phys. Rev. Lett. **86**, 1118 (2001).
[17] S. M. Bachilo, M. S. Strano, C. Kittrell, R. H. Hauge, R. E. Smalley, and R. B. Weisman, Science **298**, 2361 (2002).
[18] E. Pop, D. A. Mann, K. E. Goodson, and H. J. Dai, J. Appl. Phys. **101**, 093710 (2007).
[19] D. J. Yang, S. G. Wang, Q. Zhang, P. J. Sellin, and G. Chen, Phys. Lett. A **329**, 207 (2004).
[20] F. M. Huang, K. T. Yue, P. H. Tan, S. L. Zhang, Z. J. Shi, X. H. Zhou, and Z. N. Gu, J. Appl. Phys. **84**, 4022 (1998).
[21] H. D. Li, K. T. Yue, Z. L. Lian, Y. Zhan, L. X. Zhou, S. L. Zhang, Z. J. Shi, Z. N. Gu, B. B. Liu, R. S. Yang, H. B. Yang, G. T. Zou, Y. Zhang, and S. Iijima, Appl. Phys. Lett. **76**, 2053 (2000).
[22] N. R. Raravikar, P. Keblinski, A. M. Rao, M. S. Dresselhaus, L. S. Schadler, and P. M. Ajayan, Phys. Rev. B **66**, 235424 (2002).
[23] See EPAPS Document No. E-APPLAB-92-084801 for the G band temperature coefficient calibration data. This document can be reached through a direct link in the online article's HTML reference section or via the EPAPS homepage (http://www.aip.org/pubservs/epaps.html).
[24] M. Z. Atashbar and S. Singamaneni, Appl. Phys. Lett. **86**(12), 3112 (2005).
[25] S. Chiashi, Y. Murakami, Y. Miyauchi, and S. Maruyama, Chem. Phys. Lett. **386**, 89 (2004).